

Cosmic ray composition and energy spectrum above 1 TeV: direct and EAS measurements

A.Castellina^{a*}

^aConsiglio Nazionale delle Ricerche, Istituto di Cosmogeofisica, cs.Fiume 4, 10133 Torino, Italy

The most recent experimental results on the cosmic ray composition and energy spectrum above 1 TeV are reviewed and discussed. All data agree on the presence of the so-called “knee” at an energy $E_k \simeq 3 \cdot 10^{15} eV$; the knee is seen in all the components of the Extensive Air Showers. These results support the hypothesis of an astrophysical origin of the knee, while no new features in the hadronic interactions at high energies are envisaged. The cosmic ray composition below and above the knee region is still an open question. According to most experiments, the knee seems to be due to the light component of the primary beam, with a composition getting heavier above the knee. However, results contradicting this conclusion have to be considered and understood.

1. Introduction

The energy spectrum of cosmic rays (CR) spans a very wide energy range, with particle fluxes steeply falling more than 30 orders of magnitude. Above the solar modulation region, the spectrum can be well described by a power law, which steepens around $3 \cdot 10^{15} eV$, a feature called the “knee”, discovered in 1958 [1]; it softens again at $\simeq 10^{19} eV$, the “ankle”.

Explaining the knee feature would shed light on the CR origin and acceleration mechanism, depending on whether it is a signature of a change in the hadronic interactions at such energies or it reflects a feature of the cosmic ray spectrum, thus concerning mainly astrophysics.

Several arguments involving energetics, composition and secondary γ ray production suggest that cosmic rays at least up to the knee region are confined in the Galaxy.

The most popular theory is that of diffusive shock acceleration in Supernova remnants (SNR), that is particle acceleration by SNRs expanding supersonically in the surrounding medium.

Supernova explosions can easily account for the energy stored in galactic cosmic rays; the spectrum emerging from the SNR is of the type $E^{-2.1}$ up to a maximum energy near $10^{14} eV$ times the nuclear charge, after which it drops very rapidly.

Folding the production spectrum with the effect of diffusion through the Galaxy, and taking a trapping time varying as $E^{-0.6}$ (as found from the proportion of secondary to primary nuclei arriving to Earth), the resulting flux of CR in the Galaxy would be $\propto E^{-2.7}$, in close agreement with expectations. The maximum achievable energy is close to the knee one.

A direct evidence that the nucleonic component of CR is indeed produced in SNRs could be obtained by the observation of γ rays: the accelerated cosmic rays can in fact interact with the local interstellar matter, in this way producing γ rays by either hadronic or leptonic production.

Various experimental groups reported on TeV γ emission from supernova remnants, like SN1006, RJX1713.7-3946, Cassiopea-A (see e.g. [2] and references therein). Unfortunately in all cases the emission can be attributed to electron progenitors and no positive evidence for hadroproduction of TeV γ 's has been found yet.

Further information can be obtained from the study of the distribution of CR arrival directions. A recent compilation of the anisotropy measurements can be found in [3]; while the amplitude and phase of anisotropy data below $\simeq 2 \cdot 10^{14} eV$ are consistent and statistically accurate [4], the experimental results at higher energies are not compatible with expectations. This could mean that the diffusion model cannot be simply extrapolated to higher energies.

*E-mail: castellina@to.infn.it.

olated to these energies [5].

Various models have been put forward trying to identify the sites and mechanisms of injection of cosmic rays at higher energies, at and above the knee. If the bend in energy spectrum is related to the maximum achievable energy in the accelerator, then CR at higher energies could be powered by a reacceleration by interstellar turbulence [6], or they could be produced by Supernovae exploding in denser media (their stellar wind cavity) ([7] and references therein). On the other hand, the knee could be attributed to propagation effects. In both cases, one would expect multiple bends due to the different elements bending at fixed rigidity; the composition would become heavier above the knee. An extra-galactic origin for CR above the knee has also been proposed [8], where the accelerator sites are found in Active Galactic Nuclei and the resulting composition is getting lighter above the knee.

A completely different point of view assigns the knee to a new dramatic process of hadronic interaction which takes over around the knee energy. However, even if it is true that in the ΔE of interest we have no direct information about the hadronic interaction cross section for the secondary production relevant to the interpretation of measurements, no experimental data as far show a need for a different interaction mechanism. From the experimental point of view, what is most important in order to test the models is to measure the cosmic ray composition and energy spectrum near the energy limit of the shock models; moreover, measurements of anisotropy and secondary to primary ratio at higher energy are of utmost importance.

2. Direct measurements

Direct measurements of the relative abundances of the cosmic ray nuclei and their distribution in energy are possible only at relatively low energy: they in fact require installation of instrumentation on balloons or space shuttles flying outside the atmosphere at very high altitude. The most recent results still come from two balloon experiments, JACEE and RUNJOB, as summarised in [9,10].

The proton and Helium spectra have been measured by JACEE up to about 800 TeV [11]; no break was found in the proton one, but above 80-90 TeV the experiment does not have enough statistics to either assess or reject its presence [12].

JACEE claim for a flatter He spectrum as compared to the proton one is in agreement with SOKOL result [13], but this is not confirmed by the results by RUNJOB [14]. The JACEE group reported values are $\gamma_p = (-2.80 \pm 0.04)$ and $\gamma_{He} = (-2.68 \pm 0.06)$, while RUNJOB slopes are both $\simeq -2.80$ with an uncertainty between 10 and 20% for both protons and Helium nuclei. It should however be mentioned that the significance of the difference between the slopes for p and He is at the level of only 2σ ; on the other hand, the results from RUNJOB are based only on the 1995 and 1996 data ($\simeq 30\%$ protons and $\simeq 13\%$ He respect to JACEE data). The experimental results on the p and He slopes are of particular importance as regards the models of non linear acceleration of cosmic rays, where the injection rate is an increasing function of the primary particle rigidity [15].

The single component spectra are shown in Fig.1 and in Fig.2. The experimental results agree for what regards the iron spectrum, while RUNJOB gives a factor of 2 lower spectra for the C-N-O and Ne-Si groups. Data are all consistent with an increase of the mean logarithm of the average primary mass $\langle \ln A \rangle$ with energy, as shown in Fig.3.

It is clear that more statistics is needed above 100 TeV, and various new projects are under development. ACCESS [16] is estimated to be launched on the International Space Station in 2006. Its primary goal will be the measure of energy spectrum and composition up to $10^{15} eV$, thus testing Supernova shock acceleration models; the charge range at high energy will be $1 \leq Z \leq 28$. Three different detectors are being built for this purpose: a charge identification module, to measure the abundances of all individual elements, a transition radiation detector, to identify and measure the energy of particles with $Z \geq 2$ up to $\simeq 100 TeV/nucleon$, a calorimeter to measure the particle energies and to identify electrons.

The ATIC [17] project, in its initial design for long duration balloon flights, is devoted to study the energy spectrum of Galactic proton and helium up to $10^{14}eV$, in order give information about the proton/helium ratio, the possible dif-

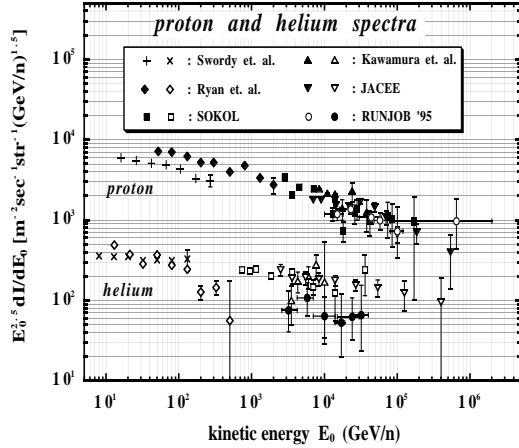


Figure 1. *Differential energy spectra for proton and helium* [10].

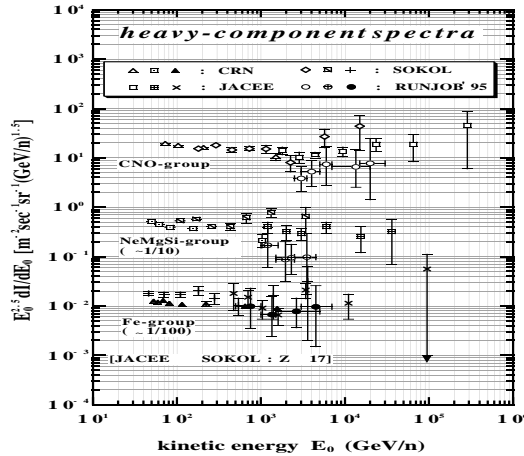


Figure 2. *Differential energy spectra for the CNO, NeMgSi and Iron groups* [10].

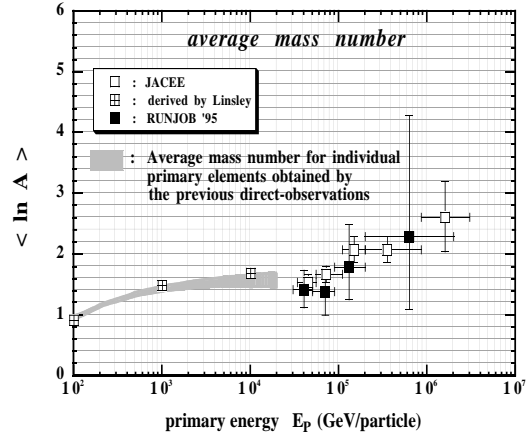


Figure 3. *Average primary mass vs primary energy from direct measurements* [10].

ference in their spectral slopes, the existence of a bend in the proton spectrum.

CREAM [18] plans to explore spectrum and composition up to $\simeq 10^{15}eV$, exploiting ultra long duration balloon flights ($\simeq 100$ days). With an exposure of $\simeq 300 m^2 sr days$, this instrument will collect $\simeq 500$ proton and helium nuclei above $10^{14}eV$, reaching $\simeq 30\%$ statistical accuracy above $10^{15}eV$.

The new Ionization Neutron Calorimeter INCA [19] proposes to study the range 0.1-10 PeV using the well known techniques of ionization and neutron monitor to measure energy and a silicon particle charge detector to determine the charge and coordinates of the primaries.

Combining different detectors, the new projects will have a very powerful tool to overcome the individual technical limitations.

3. The energy spectrum

The experimental observables which are measured in order to extract information about the energy spectrum are the charged components of showers as measured by ground based detectors with scintillator counters, muon and hadron detectors, or the Čerenkov light produced by shower

particles as they propagate through the atmosphere.

The interpretation of these ground level observations in terms of primary particle characteristics is far from straightforward, being strongly dependent on models simulating the production and propagation of particles through the atmosphere. Models in turn depend on extrapolations applied to the data on high energy particle interactions studied at accelerators; the energy region of interest is in fact much higher than that studied at accelerators, the explored kinematic region is the forward one, the collisions among nuclei make the influence of nuclear effects not negligible.

The most recent results of EAS experiments concerning the primary energy spectrum of cosmic rays are described in the following.

The electron size spectra as measured by the EAS-TOP experiment [20] are shown in Fig.4. The knee is clearly visible, and the size corresponding to the knee shifts towards lower values at increasing atmospheric depth, as expected for a knee at given primary energy [21].

The shower size at the knee decreases with increasing atmospheric depth, with an attenuation length $\Lambda_k = (222 \pm 3) g cm^{-2}$, in very good agreement with that found for the shower absorption in atmosphere; the integral intensities $I_k(\geq E_k)$ are constant within 20%. The knee in electron size is quite sharp, showing that the change in slope occurs in a limited range of N_e ($\Delta N_e/N_e \leq 25\%$).

The muon size spectra have been measured in 4 different zenith angle intervals, as one can see in Fig.5, where the change of slope is visible at all atmospheric depths despite the large statistical fluctuations. The knee, around $N_\mu^k \simeq 10^{4.65}$, is independent on the number of detected muons, being in fact visible at any core distance [22]. The integral fluxes in electron and muon size are compatible at all atmospheric depths, as expected for a feature occurring at fixed primary energy, also confirming the consistency of the whole procedure.

A further interesting result comes from the relation between the electron and muon size slopes, which can be written as $N_\mu \propto N_e^\alpha$ with $\alpha \simeq 0.75$ in all angular bins: no sudden change in the secondary production when going through the knee

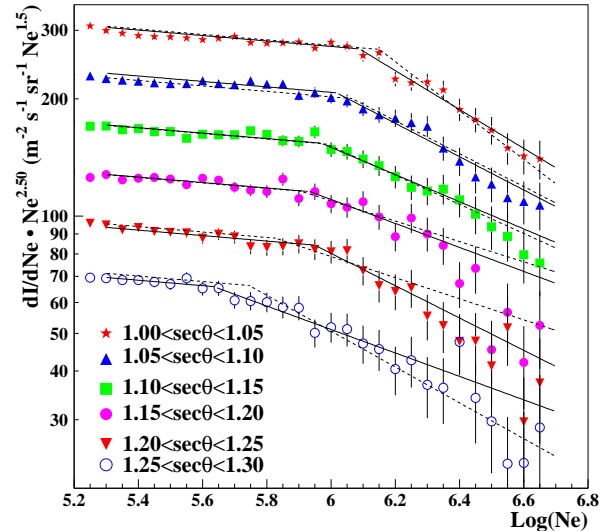


Figure 4. *Differential electron size spectrum at different zenith angles, that is different atmospheric depths, as measured by EAS-TOP. The solid lines show the results of the fitting procedure [21]; the fits represented by dashed lines were obtained requiring a constant integral flux above the knee.*

region is seen, thus showing that, at least from this point of view, no new hadronic effects is needed to explain the knee [23].

A simulation of the shower production and development in atmosphere using the CORSIKA code [24] with the HDPM interaction model allows to find the relation between shower size and primary spectrum $N_e(E_0, A) = \alpha(A_{eff})E_0^{\beta(A_{eff})}$. The effective mass A_{eff} is calculated from the extrapolation of the single nuclear spectra measured at low energies by direct measurements; above the knee, a rigidity dependent cutoff is used.

The final result is shown in Fig.6; the agreement with direct measurements at low energies and with other air shower experimental results at the highest ones is quite good. The systematic uncertainties in the energy spectrum are due to the primary composition and interaction model chosen

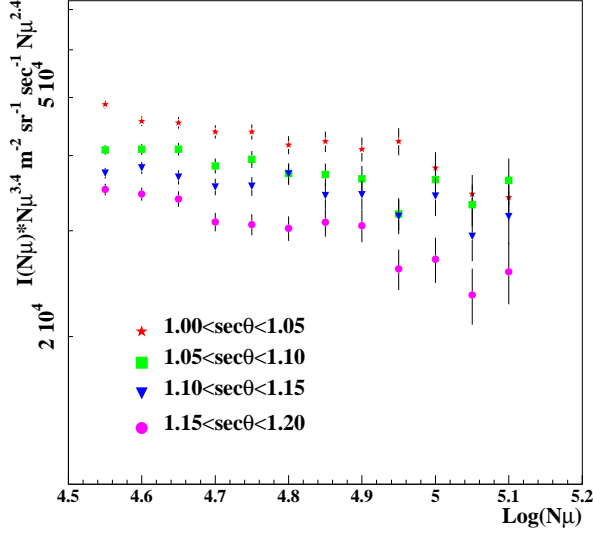


Figure 5. *Differential muon size spectrum at 4 different atmospheric depths as measured by EAS-TOP [22].*

in the calculation: the maximum difference in the determination of N_e between different interaction models and HDPM is $\simeq 10\%$; the all-particle flux obtained with “heavy” or “light” limit compositions differs by $\simeq 10\%$ from the above calculated one.

The energy spectrum is determined by CASAMIA using the muon N_μ and electron N_e^* size measurements [25]. The N_e^* indicates in this case the sum of e^+ , e^- , γ at the ground. The sizes combination $F = \log_{10}(N_e^* + \psi N_\mu)$ was found to be log-linear in E_0 and, what is most important, independent on the primary mass.

In Fig.7 this relation is shown as found from a simulation of primary protons or iron; the model used was the QGSJET one. The systematic differences in energy assignment for different primary mass A are less than 5%. The average absolute energy reconstruction errors go from $\simeq 25\%$ at $10^{14}eV$ to $\simeq 16\%$ at $\geq 10^{15}eV$.

The parameter ψ , which defines the relative weight of muons and electrons in the showers, is strongly dependent on the model used for

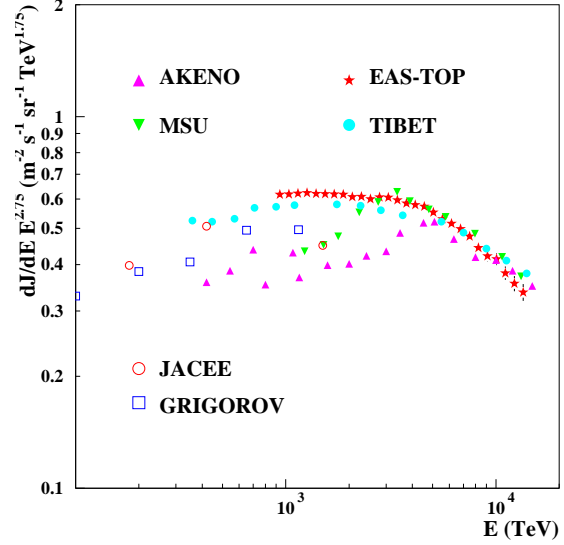


Figure 6. *Primary energy spectrum as obtained by EAS-TOP compared with other experimental results [21].*

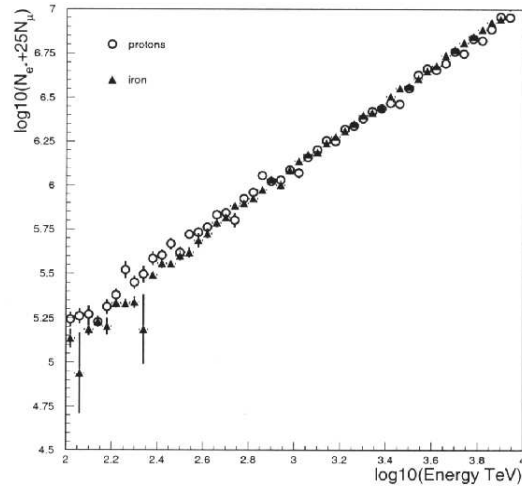


Figure 7. *$F = \log_{10}(N_e^* + \psi N_\mu)$ as a function of energy for simulated proton (open circles) and iron (black triangles) primaries [25].*

hadronic interactions, but the change in energy assignment due to this effect is claimed to be $\leq 10\%$. The mass insensitivity allows to determine the energy free of systematic effects (on the contrary, for example, if in some region the energy spectrum changes, N_e vs E also changes). The energy spectrum thus derived is shown in Fig.8; the knee is located at the same primary energy for any atmospheric depths, as expected.

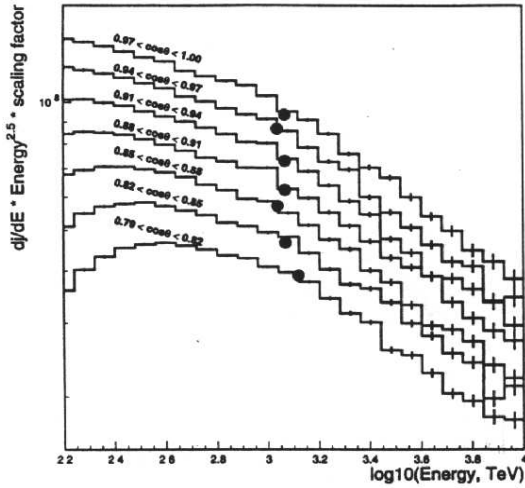


Figure 8. Primary energy spectrum as found by CASA-MIA [25].

KASCADE [26] measures all the three charged components of extensive air showers: electrons, muons and hadrons.

The knee is clearly visible in all components; for electrons and muons, the higher statistics allows to study the size at different atmospheric depths, thus finding that the size at the knee decreases at increasing atmospheric depth [27].

The primary energy spectrum can be extracted from the measured size spectra depending on the knowledge of the mass composition as obtained from the observables under investigation and on the relation between size and energy resulting from simulation.

The energy spectrum shown in Fig.9 was found

by a combined χ^2 minimisation to fit both the N_e and the N_μ truncated muon size spectra simultaneously (the truncated muon number is that found by fitting the muon lateral distribution within a limited range of 40-200 m) [28]. The evaluated size spectra are in fact the convolution of the energy spectrum and a kernel function describing the probability of a given primary to produce a shower with a certain size and which includes the parametrisations of shower fluctuations for both proton and iron primaries according to Monte Carlo. The knee is found at about 4 PeV.

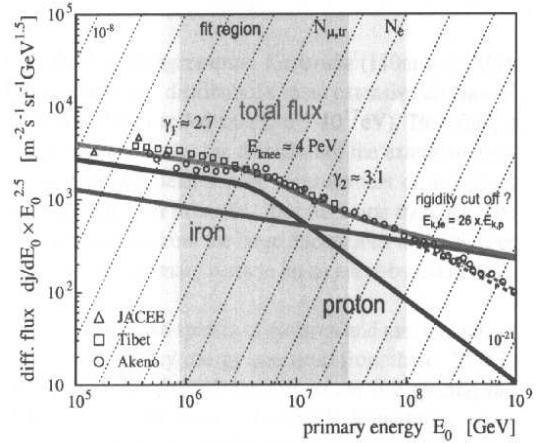


Figure 9. Primary energy spectrum by KASCADE from electron and muon size spectra [28].

In Fig.10, the energy spectrum as derived from hadronic data is also shown. The knee is again very clear, and the expectations from pure beams of protons or iron primaries are shown for comparison. Furthermore, KASCADE data show evidence of the knee also in the energy sum of hadrons in the calorimeter [29].

From muon density measurements in the multi-wire proportional chambers below the central detector [30], a subdivision of the data in “light” and “heavy” samples (according to the parameter $\text{Log } N_\mu / \text{Log } N_e$ as described in Sect.4) shows

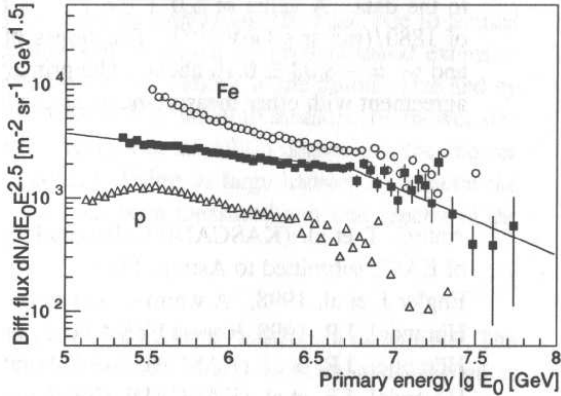


Figure 10. *Primary energy spectrum as found using KASCADE hadrons. Empty circles and triangles are the spectra from simulation of pure iron or proton primaries respectively [29].*

that the knee is strongly dominated by the light component, within a 30% uncertainty due to Monte Carlo statistics.

The broader lateral distribution of the Čerenkov light, due to the smaller absorption of photons in atmosphere, and the high photon number density, that means a better signal-to-noise ratio even for smaller arrays, are the main advantages in using Čerenkov detectors as compared to charge particle counting arrays. The most recent results from apparatus based on the detection of Čerenkov light from Extensive Air Showers come from BLANCA [31] and DICE [32], both operating at the same site and sharing some equipment with CASA.

The first one consists of 144 angle-integrating Čerenkov light detectors located in the CASA scintillator array, which provides the trigger and gives core position and shower direction. The Čerenkov lateral distribution function is measured and fitted through the expression $C(r) = C_{120}e^{-sr}$ in the inner part of the distribution ($r \leq 120$ m). The intensity at a critical radial distance of 120 m, entirely determined by density and scale height of the atmosphere, is proportional to the primary energy and the dependence on the primary mass is fully included in the slope s of the distribution, which is in fact a function of the depth of maximum development X_{max} .

DICE consists of 2 imaging telescopes of 2m diameter. What is measured is the Čerenkov light size N_γ , by summing the total amount of light at each phototube and the depth of maximum development of the shower X_{max} by fitting the shape of the light image in each telescope, with a procedure that is essentially geometrical and not depending on simulations, except for calculations to determine the angular distribution of light around the axis. The core position and shower direction are given by the CASA scintillator array.

The primary energy is estimated through a fit including geometry, N_γ and X_{max} and takes therefore into account the dependence of the lateral distribution and intensity of the Čerenkov light, at fixed primary energy, on the primary mass.

The resulting energy spectra from BLANCA and DICE are shown in Fig.11 (QGSJET model) and Fig.12 in comparison with other experimental results. The knee feature is evident in the BLANCA energy spectrum at $\simeq 3$ PeV; a 10% shift in the energy scale, which is however less than the instrumental uncertainty, is found by changing the interaction model chosen to interpret the data. The absolute calibration error results in a $\simeq 18\%$ systematic error on the energy assignment. According to DICE data, the knee is found around 3 PeV; the systematic uncertainty in the absolute flux is $\simeq 30\%$, due to the intrinsic error in the energy scale of $\simeq 15\%$.

The Čerenkov lateral distribution has also been measured by HEGRA with its AIROBICC detectors [33]. Again, the scintillator array provides the core position and arrival direction of the showers. The total primary energy can be reconstructed by the electromagnetic one, if one assumes a primary composition; however, a determination of the primary energy in a mass independent way can be obtained following the approach of Lindner [34], at the expenses of the energy resolution, which is worse than that found by the mass-dependent method and of a stronger dependence of the result on the fluctuations of X_{max} . The knee is found at about 3 PeV.

In Fig.13, the all-particle primary energy spectrum as obtained with the various experiments here described is shown. A summary of the up-to-date situation is given in Table 1. The differences

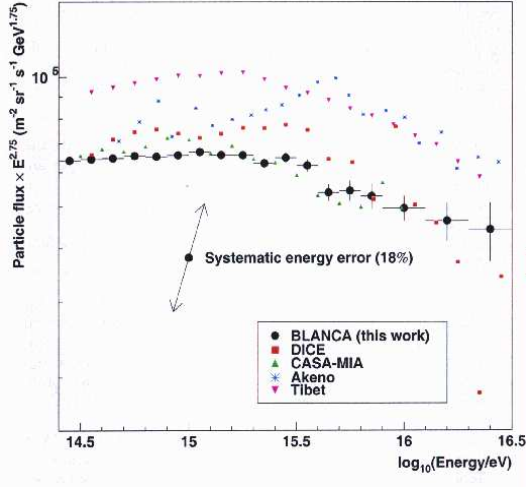


Figure 11. *Primary energy spectrum from BLANCA [31].*

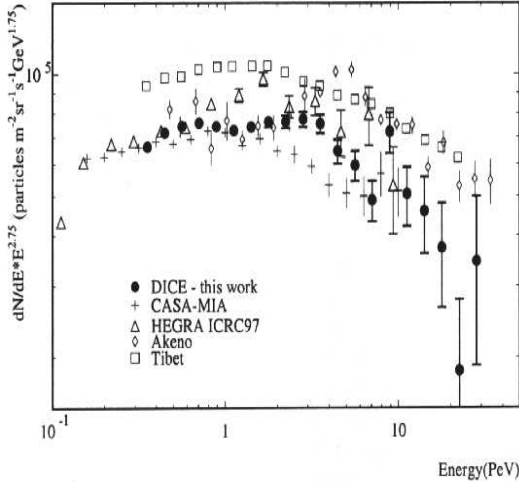


Figure 12. *Primary energy spectrum from DICE events in coincidence with CASA-MIA ([32]).*

among the quoted knee energies are mainly due to the assumed composition, which in turn depends on the observables used as will be discussed below, but the existence of the knee is clearly established between 2 and 5 PeV.

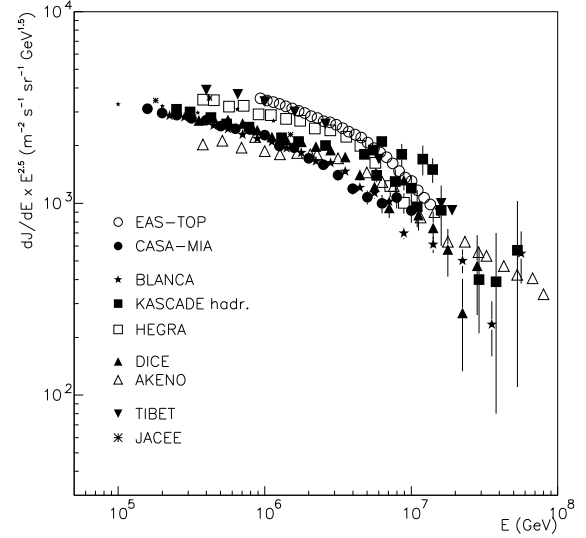


Figure 13. *All-particle primary energy spectrum from the various experiments as described in the text.*

4. Composition

The cosmic ray primary composition measurements around the knee are crucial for the understanding of the mechanisms of acceleration and the source problem.

The experimental observables we are dealing with are: a) the Čerenkov lateral distribution or the image of the Čerenkov light emitted by the shower in atmosphere; they allow to determine the depth of shower maximum X_{max} , which is a logarithmically increasing function of the primary energy. At fixed E_0 , heavier primaries are expected to interact earlier, thus giving a smaller value of X_{max} (higher in atmosphere). b) the muon and electron sizes of the showers. For a given primary energy, EAS induced by heavy primaries develop earlier in atmosphere and less energy is released in the electromagnetic component, thus producing a smaller N_e at ground level, as compared to proton showers; on the other hand, muons are produced more copiously in EAS by heavy primaries, because of the higher number

Table 1

Slopes of the energy spectrum below (γ_1) and above (γ_2) the knee. E_k is the energy at which the knee is seen (PeV).

Experiment	γ_1	γ_2	E_k (PeV)
EAS-TOP [21]	-2.76 ± 0.03	-3.19 ± 0.06	2.7 – 4.9
KASCADE [35]	-2.70 ± 0.05	-3.10 ± 0.07	4.0 – 5.0
KASCADE [29]	-2.66 ± 0.12	-3.03 ± 0.16	5.0 ± 0.5
CASA [25]	-2.66 ± 0.02	-3.00 ± 0.05	smooth
AKENO [36]	-2.62 ± 0.12	-3.02 ± 0.05	$\simeq 4.7$
TIBET [37]	-2.60 ± 0.04	-3.00 ± 0.05	smooth
TUNKA [38]	-2.60 ± 0.02	-3.00 ± 0.06	$\simeq 4.0$
BLANCA [31]	-2.72 ± 0.02	-2.95 ± 0.02	$2.0^{+0.4}_{-0.2}$
DICE [39]	$\simeq -2.7$	$\simeq -3.0$	$\simeq 3.0$
HEGRA [33]	-2.67 ± 0.03	$-3.33^{+0.33}_{-0.41}$	$3.4^{+1.3}_{-0.7}$

of low energy pions.

The EAS-TOP group studied the composition by analysing the behaviour of \overline{N}_μ as measured in vertical direction in narrow bins of N_e , corresponding to $\Delta N_e/N_e = 12\%$. The result is shown in Fig.14: data are compared with the results of a full simulation including the detector response, where the 1 TeV composition with equal slopes for all components was used, in this way assigning constant composition with energy.

The EAS-TOP data clearly suggest a growth of the mean A with energy, that is a heavier composition above the knee. A change of $\Delta \text{Log}(N_e) = 0.5$ results in a $\Delta A/A \simeq 0.4$ [40].

The “K Nearest Neighbour” test was used by CASA-MIA to study the composition [41]. Using the electron and muon densities at different distances from the core and the slope of the electron lateral distribution, samples of event for each different primary mass are generated by Monte Carlo. An experimental event is assigned to the “light primary” or “heavy primary” class by looking at the K nearest neighbours (KNN) in the plane of the used variables: the event will belong to the light primary group if e.g. more than 50% of its KNN are light primaries. Due to fluctuations, which tend to superimpose classes, only broad classes of “p-like” and “Fe-like” events can be used. The proton resemblance, defined as the average fraction of K nearest neighbours which are protons, is shown in Fig.15 for K=5, normalised

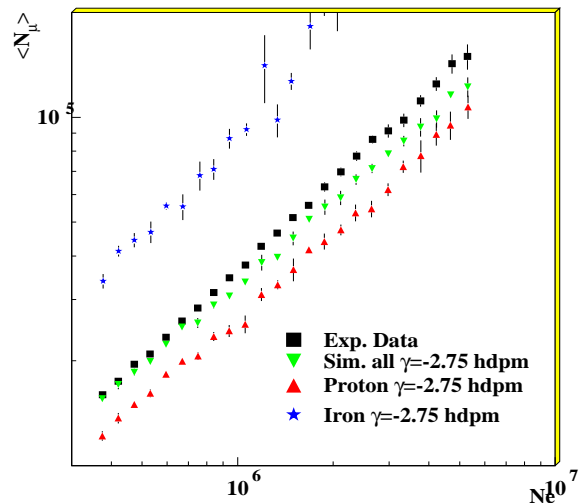


Figure 14. $\langle N_\mu \rangle$ vs N_e from EAS-TOP experimental data (full squares) as compared to a simulation with mixed composition and all components with the same slope (downward triangles), pure proton (upward triangles) and pure iron (stars) primaries [40].

such that a pure proton composition would lay along the top of the plot and a pure iron along the bottom border.

The trend towards a heavier composition above the knee is evident; a change in the hadronic in-

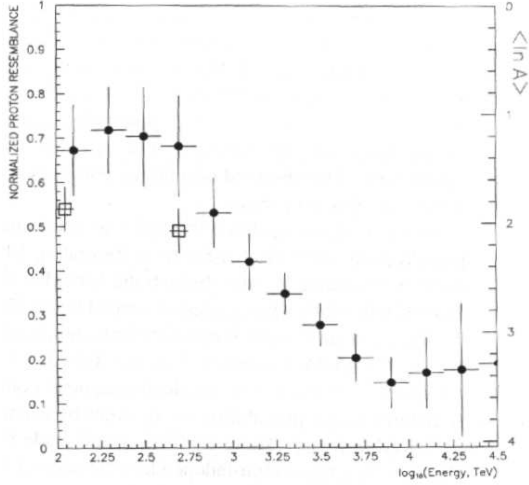


Figure 15. Normalised proton resemblance plot from CASA-MIA. The open squares give the estimated result if the composition is taken from JACEE direct measurements [41].

teraction model used in the simulation does not change the result. Classifying the events according to their probability of being light or heavy primaries and plotting the energy spectrum for the two classes separately, CASA-MIA data suggest that the knee be due to the light mass group; the spectra are consistent with the idea of cutoffs proportional to the particle rigidities.

The composition problem has been attacked by KASCADE people in a variety of ways, using different observables and analysis methods.

The most sensitive dependence on primary mass was identified in the ratio $\log N_{\mu}^{tr}/\log N_e$, which is found to be Gaussian distributed at fixed A [42]. The experimental ratio is fitted by a superposition of simulated distributions (one for each primary mass group), directly obtaining the fraction of each mass group, as shown in Fig.16 for two energy bins. The composition is dominated by the light component up to about 4 PeV, getting heavier above the knee; the analysis also proves that the composition cannot be described by a single component. The $\langle \ln A \rangle$ so obtained is shown in Fig.18.

A number of hadronic observables has also been

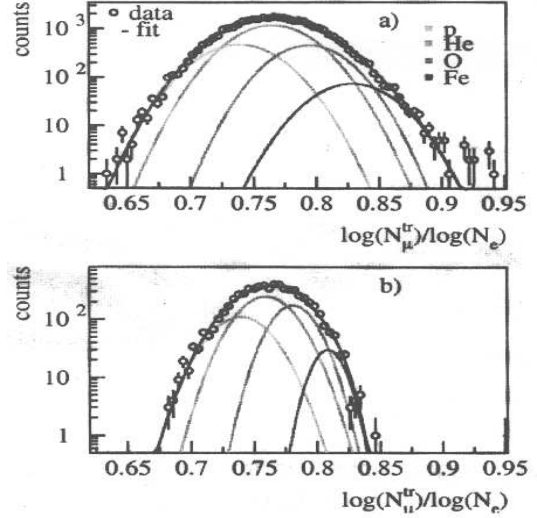


Figure 16. $\log N_{\mu}^{tr}/\log N_e$ for two of the considered energy bins: $6.2 \leq \log(E/GeV) \leq 6.3$ and $6.7 \leq \log(E/GeV) \leq 6.8$ [42].

used, such as the lateral hadron distribution, the hadron energy spectrum, the maximum hadron energy etc. in order to investigate the composition. As one can see in the world survey given in Fig.18, the hadronic data alone give a heavier composition as compared to other data.

An interesting approach was used in [43], where a multivariate analysis using all the measured components of the EAS is performed. The result shows a tendency to a lighter composition approaching the knee, followed by an increase in the average mass above it.

A comparison among the results by KASCADE shows that the absolute scale strongly depends on the observables which are used. It is clear that the balance of energy among the different components of EAS in the simulation does not reproduce the real situation; tests of the high energy interaction models are being performed [44]. In experiments like BLANCA, Spase-VULCAN [45], CACTI [46], Hegra-AIROBICC, X_{max} is measured from the slope of the Čerenkov lateral distribution, which is an almost linear function of the depth of shower maximum. This function is rather independent on the models chosen for the

description of hadronic interactions, while any interpretation of the experimental results in terms of primary composition is not.

In the case of DICE, the imaging technique allows to measure X_{max} in a rather direct way, by fitting the shape of the shower Čerenkov image in each of the 2 telescopes, knowing the arrival direction and the core position of the shower.

A survey of the results is shown in Fig.17, up to the Fly’s Eye energies (where air fluorescence is measured); the “direct” point shows the X_{max} that would be expected on the basis of balloon direct measurements [47].

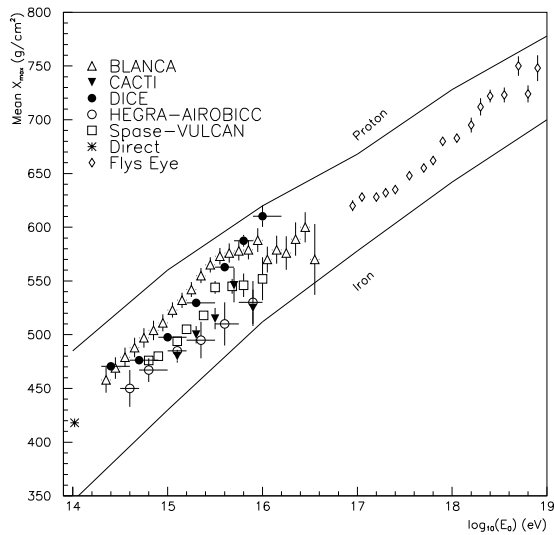


Figure 17. Mean height of shower maximum vs energy as measured by various devices. HEGRA data from [48], Fly’s Eye data from [49]. The lines show the expectations from a pure proton or iron composition using CORSIKA+QGSJET [50].

BLANCA data suggest a composition getting lighter near the knee and turning to a heavier one after the knee energy. Data from DICE require a

composition becoming progressively lighter with increasing energy.

DICE and CASA-MIA groups studied the composition problem also by means of a combination of measured parameters [32]. Two estimates of the mass have been derived, one using the X_{max} as determined by DICE and the other with N_μ and N_e by CASA-MIA, for each detected shower. The combined use of different measurements allows first of all a study of the systematics biasing the composition results; moreover, the requirement of consistency among various measurements allows to limit the range of the parameters used in the models. This analysis suggests a primary composition becoming lighter at and above the knee, not excluding however a constant composition around the knee energy.

A survey of the previously described results on primary composition in terms of $\langle \ln A \rangle$ is shown in Fig.18.

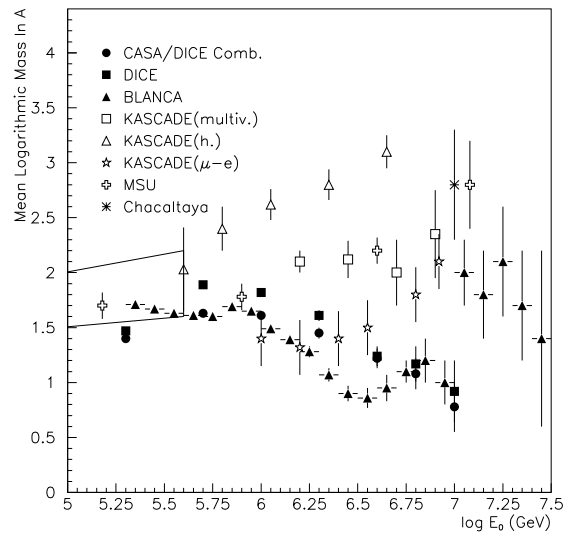


Figure 18. Mean logarithmic mass vs primary energy. The box represents the region of direct measurements [52]. MSU data from [51], Chacaltaya data from [53].

5. Conclusion

The cosmic ray energy spectrum and composition are studied with a variety of experimental techniques detecting different air shower components in the energy region above 1 TeV.

Below the knee, no new data are available and the conclusions reached by JACEE and RUNJOB experiments still hold; however new projects, planned to fly on balloons or on the Space Station, are in progress. They will surely extend the explorable energy region and the available statistics on single nuclei.

The energy spectrum has been studied in detail both by charged particles and Čerenkov light ground arrays and some firm conclusions were reached: all data agree on the existence of the knee in the primary energy spectrum of cosmic rays at an energy $\simeq 3 - 4$ PeV. The bend has been seen in all shower components, thus supporting an astrophysical interpretation of the knee as opposite to that of a change in the hadronic interaction picture at these energies. All results agree to attribute the knee to the medium-light mass primaries.

Progress has been made as regards the mass composition. Almost all the ground array results show an increase in the primary mean logarithmic mass above the knee, even if the absolute scale can be quite different. There are however contradicting results coming from experiments relying on the Čerenkov light detection from Air Showers; the differences in the measure of X_{max} are however quite big.

It is very important to study in detail the systematics which could bias the results; the combined use of different observables and the comparison among various data sets can help in this task. The different sensitivity to composition of the various used observables, the methods employed to determine the primary energy and the problems found in the models used in the simulations could explain the spread in the results which is apparent in Fig.18.

Acknowledgements

I would like to thank my friends G.Navarra, B.Alessandro and A.Chiavassa for the interesting

and useful discussions which were the basis of this paper. Sincere thanks also to all my Brazilian friends, for their warm hospitality during my stay in Campinas.

REFERENCES

1. Kulikov G.V. and Khristiansen G.B., *Sov.Phys. JETP* **8** (1959) 41.
2. Weekes T., *6th Workshop on GeV-TeV Gamma-Ray Astrophysics : Toward a Major Atmospheric Cherenkov Telescope VI*, Snowbird, UT, USA, 13-16 Aug 1999 Ed. by Dingsus, B.L.; astro-ph/9910394.
3. Clay R.W. et al., *Proc.25th Int.Cosmic Ray Conf.*, **4**, Durban (1997) 185.
4. Aglietta M. et al., *Ap.J.*, **470** (1996) 501.
5. Hillas A.M., *Proc.26th Int.Cosmic Ray Conf.*, **4**, Salt Lake City (1999) 225.
6. Seo E.S. and Ptuskin V.S., *Astrophys.J.*, **431** (1994) 705.
7. Biermann P.L. et al., "The Central Parsecs of the Galaxy", ASP Conf.Series, Vol. 186. Ed. by H.Falcke, A.Cotera, W.J. Duschl, F.Melia, M.J.Rieke (1999) 543.
8. Protheroe R.J. et al., *Phys.Rev.Lett.* **69** (1992) 2885.
9. Watson A., *Proc.25th Int.Cosmic Ray Conf.*, Rapporteur Talk, Durban (1997).
10. Shibata T., *Nucl.Phys.B, Proc.Suppl.*, **75A** (1999) 22.
11. Asakimori K. et al., LSU Space Science/Part.Astroph.Prep.11/3/97.
12. Cherry M., *Proc.26th Int.Cosmic Ray Conf.*, **3**, Salt Lake City (1999) 187.
13. Ivanenko I.P. et al., *Proc.23th Int.Cosmic Ray Conf.*, **2**, Calgary (1993) 17.
14. Apanasenko A.V. et al., *Proc.26th Int.Cosmic Ray Conf.*, **3**, Salt Lake City (1999) 163.
15. Berezhko E.G., Ksenofontov L.T., *Proc.26th Int.Cosmic Ray Conf.*, **4**, Salt Lake City (1999) 381.
16. Wefel J.P. et al., *Proc.26th Int.Cosmic Ray Conf.*, **5**, Salt Lake City (1999) 84. See also <http://www701.gsfc.nasa.gov/access/access.htm>.
17. Guzik T.G. et al., *Proc.26th Int.Cosmic Ray Conf.*, **5**, Salt Lake City (1999) 9.
18. Seo E.S. et al., *Proc.26th Int.Cosmic Ray*

- Conf.*, **3**, Salt Lake City (1999) 207.
19. INCA Coll., *Proc.26th Int.Cosmic Ray Conf.*, **3**, Salt Lake City (1999) 215.
 20. Aglietta M. et al., *Nucl.Instr.Meth.* **A336** (1993) 310.
 21. Aglietta M. et al., *Astrop.Phys.* **10** (1999) 1.
 22. Aglietta M. et al., *Nucl.Phys.B (proc.Suppl.)*, **85** (2000) 318.
 23. Aglietta M. et al., *Nucl.Phys.B, Proc.Suppl.* **75A** (1999) 251.
 24. D.Heck et al., Report FZKA 6019, Forschungszentrum Karlsruhe (1998).
 25. Glasmacher M.A.K. et al., *Astrop.Phys.* **10** (1999) 291.
 26. Klages H.O. et al., *Nucl.Phys.B Proc.Suppl.* **B52** (1997) 92.
 27. Kampert K.H. et al., "Second Meeting on New Worlds in Astroparticle Physics", Univ.of Algarve, Faro, Poretugal (1998).
 28. Glasstetter R. et al., *Proc.26th Int.Cosmic Ray Conf.*, **1**, Salt Lake City (1999) 222.
 29. Hörandel J.H. et al., *Proc.26th Int.Cosmic Ray Conf.*, **1**, Salt Lake City (1999) 337.
 30. Haungs A. et al., *Proc.26th Int.Cosmic Ray Conf.*, **1**, Salt Lake City (1999) 218.
 31. Fowler J.W. et al., *astro-ph/0003190*.
 32. Swordy S.P., Kieda D.B., *Astrop.Phys.* **13** (2000) 137.
 33. Röhring A. et al., *Proc.26th Int.Cosmic Ray Conf.*, **1**, Salt Lake City (1999) 214.
 34. Lindner A., *Astrop.Phys.* **8** (1998) 235.
 35. Kampert K.H. et al., *Proc.26th Int.Cosmic Ray Conf.*, **3**, Salt Lake City (1999) 159.
 36. Nagano M. et al., *J.Phys.G* **10**, **9** (1984) 1295.
 37. Amenomori M. et al., *Astrophys.J.* **461** (1996) 408.
 38. Gress O.A. et al., *Proc.25th Int.Cosmic Ray Conf.*, **4**, Durban (1997) 129.
 39. Kieda D.B. and Swordy S.P., *Proc.26th Int.Cosmic Ray Conf.*, **3**, Salt Lake City (1999) 191.
 40. Aglietta M. et al., *Proc.26th Int.Cosmic Ray Conf.*, **1**, Salt Lake City (1999) 230.
 41. Glasmacher M.A.K. et al., *Astrop.Phys.* **12** (1999) 1.
 42. Weber J.H. et al., *Proc.26th Int.Cosmic Ray Conf.*, **1**, Salt Lake City (1999) 341.
 43. Roth M. et al., *Proc.26th Int.Cosmic Ray Conf.*, **1**, Salt Lake City (1999) 333.
 44. Antoni T. et al., *J.Phys.G:Nucl.Part.Phys.* **25** (1999) 2161.
 45. Dickinson J.E. et al., *Nucl.Instr.Meth.*, **A440**, (2000) 114.
 46. Paling S. et al., *Proc.25th Int.Cosmic Ray Conf.*, **5**, Durban (1997) 253.
 47. Swordy S.P., *Proc.23th Int.Cosmic Ray Conf.*, Invited and Rapporteur, Calgary (1993) 243.
 48. Röhring A. et al., *Proc.23th Int.Cosmic Ray Conf.*, **3**, Salt Lake City (1999) 152.
 49. Bird D. et al., *Phys.Rev.Lett.*, **71**, (1993) 3401.
 50. Pryke C., *Auger GAP Note 98-035*, FNAL (1998).
 51. Fomin Yu.A. et al., *Proc.16th ECRS*, Alcala (1998) 261.
 52. Wiebel-Sooth B., "All particle Energy Spectrum measured at HEGRA", Thesis, **WUB-Dis-98-9**, Wuppertal Univ. (1998).
 53. Aguirre C. et al., *SCAN-0009225*, subm.to Phys.Rev.D (2000).